Research Article | Vol. 29, No. 23 / 8 Nov 2021 / Optics Express 37091
Optics EXPRESS

Accurate measurement of the photonic crystal slab period using diffraction in the Littrow configuration

JOHN LAWALL,[1,3] YILIANG BAO,[1,2,4] AND JASON J. GORMAN[1,5]

[1]*Physical Measurement Laboratory, National Institute of Standards and Technology, Gaithersburg, Maryland 20899, USA*
[2]*Theiss Research, La Jolla, CA 92037, USA*
[3]*john.lawall@nist.gov*
[4]*yiliang.bao@nist.gov*
[5]*jason.gorman@nist.gov*

Abstract: Photonic crystal slab devices with subwavelength periods can be tailored to provide remarkable functionality, such as ultrahigh reflectivity in a structure only 200 nm in thickness. Accurate measurement of the characteristics of these structures is essential to compare their performance to theoretical expectations and to better understand the origin of unexpected behavior. In this work, we present a simple non-invasive method employing diffraction of a visible wavelength reference in the Littrow configuration for measuring the period of a photonic crystal slab. We have measured periods of our devices with uncertainty below 0.5 nm and expect that the uncertainty could easily be improved by an order of magnitude. In addition to facilitating development, our approach can be used to explore possible variations in the period of the photonic crystal due to its operating environment and aging.

1. Introduction

Two-dimensional photonic crystal slabs and membranes [1,2] have been widely used as high-reflectivity mirrors [3–5] and optical filters [6,7] and in such diverse areas as cavity optomechanics [8,9], chip-based lasers [10,11], and sensing [12,13]. The optical properties of a photonic crystal slab are directly related to the critical dimensions (period, hole radius, and thickness) of the crystal. Deviations from the crystal design values at the level of nanometers can adversely affect the achievable reflectivity and the center frequencies for bandpass regions [4]. These deviations are caused by a combination of lithography and etch processes during fabrication, and in some cases, can be due to residual stress that stretches the crystal, as found in silicon nitride membranes [8,9]. For example, electron beam lithography can result in variation in the period of repeating structures on the order of several nanometers [14], and the situation can be significantly worse when using stepper-based optical lithography due to photomask inaccuracies and distortion in the optics of lithography tools.

Given the importance of the crystal period, or lattice spacing, methods for measuring the period with high accuracy in fully fabricated structures are needed; such measurements can then be used to optimize fabrication and achieve higher optical performance. The conventional approach to measuring the period of a photonic crystal slab is scanning electron microscopy (SEM), due to its high resolution, wide availability in nanofabrication facilities and ease of use. There are several factors, however, that limit its effectiveness for photonic crystals. First, the accuracy for measuring the period of repeating microstructures using a metrology-grade SEM with an integrated laser interferometer is typically on the order of tens of nanometers [15], and can be substantially worse for more typical instruments found in nanofabrication facilities. For example, the accuracy of a typical SEM measurement was found to be around 1 % when measuring nanostructures using several different magnifications [16]. Second, the dielectric materials most often used for photonic crystals are prone to charging and image distortion while

#438308 https://doi.org/10.1364/OE.438308
Journal © 2021 Received 4 Aug 2021; revised 12 Oct 2021; accepted 13 Oct 2021; published 25 Oct 2021

Optics EXPRESS

imaging with an SEM, adding to the uncertainty of dimensional measurements. Finally, imaging with an SEM can cause hydrocarbon deposition on the surface of the photonic crystal [17], which can reduce reflectivity and increase optical absorption.

We are thus motivated to consider optical alternatives to the SEM. Due to the importance of diffraction gratings in instrumentation, a substantial literature concerning accurate characterization of their periods exists. Typically, laser light of a known wavelength is directed on the sample, and diffraction is observed in one or two orders. Many use a Littman configuration, in which the grating is fixed and an auxiliary mirror is rotated on a precision rotation stage in order to retroreflect the diffracted beams; the grating period can then be inferred from the laser wavelength and a set of angular measurements. In its simplest implementation, this approach uses a single laser wavelength and the zeroth-order and first-order diffractions [18]. Refinements include using two laser wavelengths [19] and using the zeroth-order and two higher-order diffractions [20]. Similar techniques can be adopted for the measurement of the period of two-dimensional photonic crystal slabs. In this work, we demonstrate use of the Littrow diffraction configuration to measure the period of a photonic crystal relative to a reference laser, employing up to eight different nontrivial diffracted orders. We have measured the periods of photonic crystals with square and hexagonal lattices with an uncertainty of ≈ 0.3 nm with this technique, more than an order of magnitude better than we are able to measure with our SEM.

2. Littrow diffraction

Diffraction in Littrow configuration is a technique widely used with diode lasers to force lasing at a specific wavelength related to the angular orientation of a grating [21]. When light of wavelength λ is incident on a diffraction grating in a plane perpendicular to the grating lines, with an angle θ_i to the normal, diffracted beams are observed at angles θ_d given by

$$\sin\theta_d - \sin\theta_i = \frac{\lambda}{a}m, \tag{1}$$

where a is the grating period and m is an integer [22]. The case $m = 0$ corresponds to specular reflection, for which $\theta_d = \theta_i$. The Littrow configuration involves choosing an incident angle such that $\theta_d = -\theta_i$, giving

$$\sin\theta_d = \frac{\lambda}{2a}m. \tag{2}$$

The diffracted beam corresponding to order m then exactly retraces the incident beam.

In this work, we employ the Littrow configuration with a 2D photonic crystal slab to determine the crystal period a in terms of a known laser wavelength λ, as shown in Fig. 1. For photonic crystal slabs with a 2D lattice structure, however, the diffraction Eq. (1) must be generalized. Fig. 2 shows diffraction patterns obtained in transmission with normally incident light from a helium-neon laser ($\lambda = 632.8$ nm), for photonic crystal slabs with square and hexagonal lattices. A similar pattern is observed in reflection. It is clear that the realization of Littrow configuration will require a condition on the azimuthal angle ϕ of the sample relative to the incoming wavevector as well as the polar angle θ. The most straightforward way to derive the necessary conditions on ϕ and θ is through use of the reciprocal lattice.

Given a spatial lattice defined by $\mathbf{R}_{mn} = m\mathbf{a}_1 + n\mathbf{a}_2$, where m and n are integers and $\mathbf{a}_1$ and $\mathbf{a}_2$ are basis vectors, the reciprocal lattice [23,24] is the set of vectors $\mathbf{G}_{mn}$ such that $\mathbf{G}_{mn} \cdot \mathbf{R}_{mn} = 2\pi N$ for integer values of N. Its importance here is that when scattering off a photonic crystal slab, the component of the wavevector in the plane of the photonic crystal must change by a reciprocal lattice vector [1,24]. As shown in Fig. 1, we take the photonic crystal to lie in the xy plane and the incident beam in the xz plane: $\mathbf{k}_{inc} = k(\sin\theta\,\hat{x} + \cos\theta\,\hat{z})$, where $k = 2\pi/\lambda$. The allowed diffracted wavevectors are $\mathbf{k}^{mn} = k\sin\theta\,\hat{x} + \mathbf{G}_{mn} + k_z^{mn}\hat{z}$, where k_z^{mn} is determined by the

Optics EXPRESS

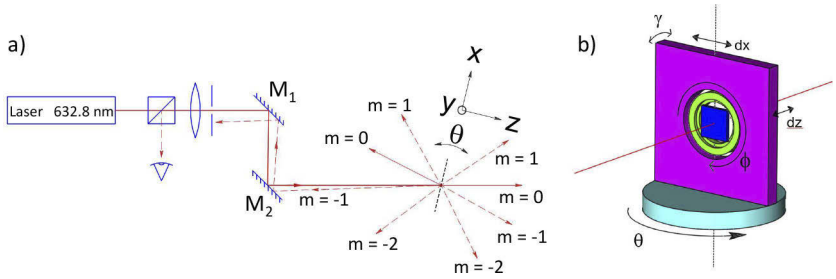

Fig. 1. **a)** The sample is mounted on a rotation stage that can be rotated by an angle θ around the vertical axis. Light from a helium-neon laser is brought to a weak focus and impinges at its waist on the sample; diffraction is observed both in transmission and reflection. As the sample is rotated, the various orders of diffraction are sent directly back to the laser when the Littrow condition is met. **b)** The sample mount requires four degrees of freedom on top of the rotation stage; two displacements dx and dz, and two angles γ and ϕ. The linear displacements are used to ensure that the sample stays centered on the rotation axis as θ is swept. The angle γ is set so that the specular reflection is perpendicular to the rotation axis for all θ, and the angle ϕ is set so that the diffracted beams are also perpendicular to the rotation axis. In the interest of clarity, diffracted beams are not shown.

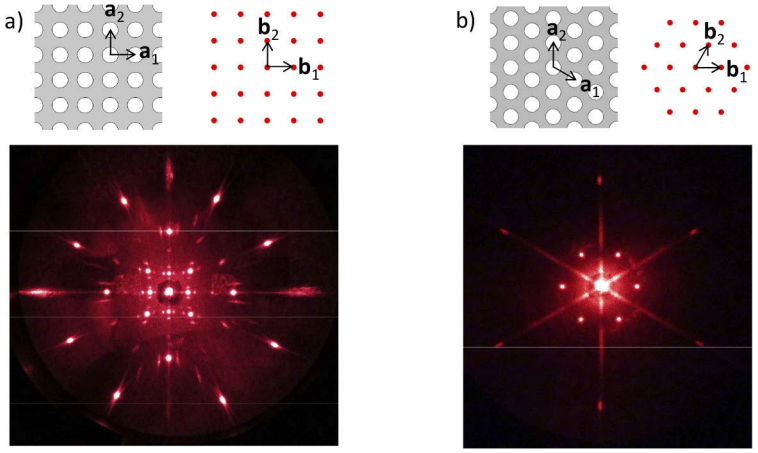

Fig. 2. **a)** Diffraction pattern observed from a photonic crystal slab with a square lattice. **b)** Diffraction pattern observed for a photonic crystal slab with a hexagonal lattice. In both cases the laser wavelength is $\lambda = 632.8$ nm. The patterns were photographed by allowing the transmission through the photonic crystal to fall on a thin, tautly stretched rubber screen, and photographing the screen from behind. The direct transmission was attenuated by means of a small dot of paint on the center of the screen. The hexagonal photonic crystal was actually embedded in a hexagonal *phononic* crystal with a period ($\approx 150\mu$m) about 100 times larger than the photonic crystal, leading to the "halo" and streaks in the image. **Top:** Illustrations of the spatial lattice with basis $\mathbf{a}_1, \mathbf{a}_2$, and corresponding reciprocal lattice basis $\mathbf{b}_1, \mathbf{b}_2$, for each case.

Optics EXPRESS

condition $|\mathbf{k}^{mn}|^2 = k^2$. Transmission and specular reflection are given by $m = n = 0$, for which $k_z^{mn} = \pm k \cos\theta$.

The Littrow condition that diffracted order mn return directly toward the source is $\mathbf{k}^{mn} = -\mathbf{k}_{inc}$, giving

$$2k \sin\theta\, \hat{x} + \mathbf{G}_{mn} + k_z^{mn}\hat{z} + k\cos\theta\, \hat{z} = 0. \tag{3}$$

This is actually a set of three coupled equations; taking scalar products with unit vectors $\hat{x}$ and $\hat{y}$ gives

$$\sin\theta = -\frac{\mathbf{G}_{mn}\cdot\hat{x}}{2k}, \tag{4}$$

$$\mathbf{G}_{mn}\cdot\hat{y} = 0. \tag{5}$$

The first of these equations determines the polar angle θ, and the second determines the azimuthal angle ϕ. To go further, we must make a specific choice of lattice. In this work, we treat the cases of lattices with square and hexagonal symmetry.

We start with the square lattice for simplicity. A two-dimensional square lattice with period a may be defined by primitive lattice vectors $\mathbf{a}_1 = a\hat{x}$ and $\mathbf{a}_2 = a\hat{y}$. The corresponding reciprocal lattice is also a square lattice, whose basis may be taken to be $\mathbf{b}_1 = (2\pi/a)\hat{x}$ and $\mathbf{b}_2 = (2\pi/a)\hat{y}$. The set of all reciprocal lattice vectors is given by $\mathbf{G}_{mn} = m\mathbf{b}_1 + n\mathbf{b}_2$, where m and n are integers; the square lattice and corresponding reciprocal lattice are indicated in Fig. 2. If the photonic crystal is rotated by an angle ϕ about the z-axis, the basis of the reciprocal lattice becomes

$$\mathbf{b}_1 = \frac{2\pi}{a}(\cos\phi\hat{x} + \sin\phi\hat{y}), \tag{6}$$

$$\mathbf{b}_2 = \frac{2\pi}{a}(-\sin\phi\hat{x} + \cos\phi\hat{y}). \tag{7}$$

Inspection of the diffraction pattern on the left in Fig. 2 suggests that the Littrow condition can be met for azimuthal angles $\phi = N\pi/2$ and $\phi = \pi/4 + N\pi/2$, as well as certain other discrete angles. The choice of these angles ϕ is readily seen to satisfy (5) when the $\mathbf{b}_i$ from (6) and (7) are used. The diffraction condition (4) on θ is then found to be

$$\sin\theta = \frac{\lambda}{2a}m; \quad \phi = 0, \tag{8}$$

$$\sin\theta = \frac{\lambda}{\sqrt{2}\,a}m; \quad \phi = \pi/4. \tag{9}$$

(Here and henceforth we suppress angles that are obviously related by symmetry, in this case rotations of multiples of 90°). The condition for $\phi = 0$ is seen to be the same as the Littrow condition (2) for a simple 1D grating, but the condition for $\phi = \pi/4$ is different. Diffraction will occur for all integral orders m such that $|\sin\theta| \leq 1$. For a square lattice with period a, then, the incident wavelength must be less than $2a$ for the method to be applicable.

For a hexagonal photonic crystal, the spatial and reciprocal lattices are also shown in Fig. 2 for the case $\phi = 0$. The reciprocal lattice is also hexagonal, but rotated from the spatial lattice by 30°. For general azimuthal angle ϕ, it is generated by basis vectors

$$\mathbf{b}_1 = \frac{2\pi}{a}\frac{2}{\sqrt{3}}(\cos\phi\hat{x} + \sin\phi\hat{y}), \tag{10}$$

$$\mathbf{b}_2 = \frac{2\pi}{a}\frac{2}{\sqrt{3}}(\cos(\pi/3+\phi)\hat{x} + \sin(\pi/3+\phi)\hat{y}). \tag{11}$$

Once again, inspection of Fig. 2 suggests that the Littrow condition can be met for azimuthal angles $\phi = 0$ and $\phi = \pi/6$, which indeed are allowed by (5) in conjunction with (10) and (11).

Optics EXPRESS

Application of (4) then yields the diffraction conditions

$$\sin\theta = \frac{\lambda}{\sqrt{3}\,a}m; \quad \phi = 0, \tag{12}$$

$$\sin\theta = \frac{\lambda}{a}m; \quad \phi = \pi/6. \tag{13}$$

From (12) it is clear that the incident wavelength must be less than $\sqrt{3}\,a$ for the method to be applicable to a hexagonal lattice.

For completeness, we note that other azimuthal angles ϕ enabling the Littrow criterion to be met exist. For the square lattice, for example, we find from (5)

$$\phi = \tan^{-1}\left(\frac{n}{m}\right) \tag{14}$$

for integral m and n. Taking $(n, m) = (1, 2)$ and $(n, m) = (2, 1)$ yields $\phi = 0.46$ rad (27°) and $\phi = 1.1$ rad (63°), corresponding to diffraction orders readily visible in Fig. 2. The corresponding diffraction condition on θ can be found with (4).

3. Setup

The experimental setup is shown in Fig. 1. Light from a wavelength-stabilized helium-neon laser is weakly focused by a lens, passes through a diaphragm, and is directed by means of two mirrors to the sample mount. The two mirrors provide the four degrees of freedom necessary to bring the waist of the beam onto and perpendicular to the sample. At normal incidence, defining $\theta = 0$, a fraction of the incident light is returned to the laser, passes through the diaphragm, and after reflection by a beamsplitter is captured by a photodetector. As the sample is rotated, the nontrivial diffracted orders also return through the diaphragm when the Littrow condition is met. By rotating the sample and measuring the angles of Littrow diffraction, the period of the grating can be determined with an uncertainty dominated by the accuracy of the angular measurements.

The samples used in this study were membranes of low-stress silicon nitride, etched with arrays of air holes defined by means of electron beam lithography. One sample had a photonic crystal patterned in a square lattice over a circular domain of diameter 300 μm. The other sample had a photonic crystal with a hexagonal lattice, patterned over a circle 60 μm in diameter on a "pad" of a much larger hexagonal *phononic* crystal with a nominal period of 144 μm. Diffraction from the phononic crystal of the tail of the Gaussian beam incident on the sample is responsible for the halo and streaks seen in Fig. 2(b). The sample with the square lattice was 560 nm in thickness with holes of radius $r \approx 540$ nm, and the sample with the hexagonal lattice was 220 nm in thickness with holes of radius $r \approx 460$ nm; these parameters affect the relative intensities of the diffracted orders at visible wavelengths, but as long as the orders can be detected, the diffraction efficiency is not of importance.

To ensure that the sample remains in the laser focus as it is rotated, the sample is mounted to the rotation stage with four additional degrees of freedom, as illustrated in Fig. 1(b). These correspond to the two linear and two angular degrees of freedom required to ensure that the sample is centered on and aligned with the rotation axis of the stage determining the angle θ. The pitch angle γ is easily set by forcing the specular reflection from the sample to come back to the same vertical position (eventually directly back toward the laser) when the angle θ is rotated by 180°. Similarly, the horizontal sample position dx is set, by means of an iterative procedure involving the horizontal axis of mirror M2, in order that the sample remains centered on the laser focus when θ is rotated by 180°. The horizontal sample position dz is set so that the sample remains within the laser focus for angles beween 0° and 180°; otherwise, the diffracted orders will vanish. Degrees of freedom γ and dz are easily obtained by use of a standard three-axis

Optics EXPRESS

mirror mount; dx requires an additional 1D positioner or a lens/mirror mount providing this degree of freedom as well. Finally, the azimuthal angle ϕ must be set so that diffraction occurs in the horizontal plane. The entire alignment procedure can typically be accomplished in a matter of minutes if the operator is attentive to the purpose of each degree of freedom.

4. Results

For the square lattice, we measured Littrow diffraction angles θ for the azimuthal angle $\phi = 0$, corresponding to the orientation shown in Fig. 2. For the hexagonal lattice, we employed both the azimuthal angle $\phi = 0$, as shown in Fig. 2, and $\phi = \pi/6$ (sample rotated by 30°). In some cases, we established retroreflection by capturing the retroreflected light on a photodetector as discussed earlier, and in some cases we simply observed the retroreflected beam on the diaphragm shown in Fig. 1 by eye. Typical measurements are shown in Fig. 3(a). The data points in green are measurements of the square lattice for orders $-4 \le m \le 4$; higher orders are forbidden. These measurements were made with the photodetector shown in Fig. 1. The data points in red are measurements of the hexagonal lattice for $\phi = 0$; here only orders $-3 \le m \le 3$ are allowed. When the sample is rotated by $\phi = \pi/6$, only orders $-2 \le m \le 2$ are allowed, and the data points are shown in blue. With the hexagonal lattice the Littrow diffraction angles were established by observing the retroreflected beam on the diaphragm by eye. The diffracted beams for $\phi = \pi/6$, $m = \pm 2$ were very weak and difficult to observe, but all other diffracted beams were readily seen.

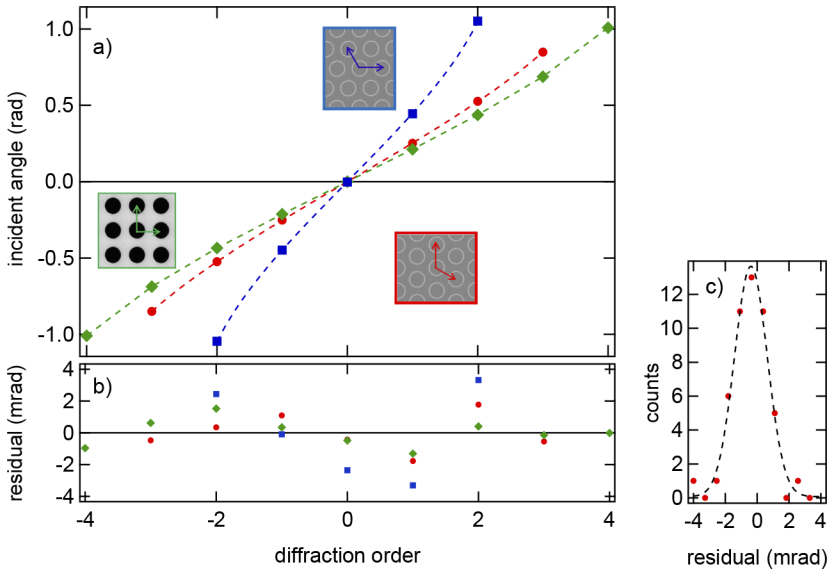

Fig. 3. **a)** Measured angles of Littrow diffraction orders and curve fits. Green diamonds refer to measurements made with a square lattice, for azimuthal angle $\phi = 0$ and fit to (8). Red circles refer to a hexagonal lattice for $\phi = 0$ fit to (12), and blue squares refer to the same hexagonal lattice rotated by $\phi = \pi/6$, fit to (13). The angle of normal incidence was a fit parameter and has been subtracted here. Error bars, corresponding to the uncertainty reading the rotation stage, are too small to see. **b)** Residuals from the fits. **c)** Histogram of the residuals from 49 measurements of the hexagonal lattice with $\phi = N\pi/3$, $0 \le N \le 6$, along with a fit to a Gaussian distribution. The standard deviation of the residuals is 1.2×10^{-3} rad, somewhat below the resolution (5' = 1.45×10^{-3} rad) of the rotation stage.

Optics EXPRESS

For the purpose of curve fitting, (8) is replaced by

$$\theta = \theta_0 + \sin^{-1}\left(\frac{1}{2}\frac{1}{(a/\lambda)}m\right), \tag{15}$$

where θ_0 and a/λ are fit parameters. Equations (12) and (13) are treated similarly. The results of these fits are shown with the dashed lines, where the angle θ_0 has been subtracted off in all cases. Figure 3(b) shows the residuals $\delta\theta_m = \theta_m^{measured} - \theta_m^{fit}$ from the fits. For the data sets shown in green and red, the characteristic size of the residuals is similar, suggesting that the measurement uncertainty is limited by how well we can read the rotation stage, rather than the method (detector or eye) used to determine exact retroreflection. The residuals for the data set shown in blue are somewhat larger, reflecting the greater uncertainty, as suggested above, in establishing retroreflection of the orders $m = \pm 2$.

The uncertainties in the derived fit parameters are of course related to the uncertainties associated with the individual data points. Figure 3(c) shows a histogram of the residuals from 49 measurements of the hexagonal lattice, as discussed below, along with a fit to a Gaussian distribution. The standard deviation of the residuals is $\sigma_{resid} = 1.2 \times 10^{-3}$ rad, but the residuals actually slightly understate the measurement uncertainty. The reason is that they are obtained by forcing a fit to a function that minimizes the sum of the squares of the residuals, rather than the "true" (but unknown) function. A detailed analysis, based on the fact that we are fitting seven data points with two adjustable parameters, shows that the standard deviation σ_θ of each point is related to the standard deviation σ_{resid} of the residuals by $\sigma_\theta^2 = (7/5)\sigma_{resid}^2$. Equivalently, $\sigma_\theta = 1.4 \times 10^{-3}$ rad is the standard deviation associated with each angular measurement. This is indeed very close to the manufacturer's quoted resolution (5' $= 1.45 \times 10^{-3}$ rad) of the rotation stage.

We are now in a position to make meaningful determinations of the lattice period by means of fits of the sort shown in Fig. 3. As a first example, for the sample with a square lattice whose diffraction measurement is shown in the green curve in Fig. 3, we measured a lattice constant of $a/\lambda = 2.3635(13)$. Here and henceforth, the uncertainty represents one standard deviation in the fit parameter as obtained by the curve fitting routine. One month later, after moving to other structures on the chip and returning to this one, we repeated the measurement and found $a/\lambda = 2.3634(13)$. In the former case, the determination of the retroreflection condition was made by eye on the diaphragm, and in the latter case it was made using a photodiode as shown in Fig. 1. The agreement was perhaps fortuitous, but it indicates the robustness of the method. Taking the laser wavelength to be $\lambda = 632.816$ nm (the contribution of the wavelength uncertainty from the stabilized laser is completely negligible), we infer a lattice period of $a = 1495.6(3)$ nm.

In another series of measurements, we repeated the determination of the period of the hexagonal structure for all of the nominally equivalent sample azimuthal angles $\phi = N\pi/3$, for $0 \le N \le 6$. We note parenthetically that the sample underwent translation in the xy plane as it was rotated, since it was not mounted at the exact center of the stage determining ϕ; consequently, the alignment procedure described above was used repeatedly. The 49 (7×7) angular measurements made for this series were in fact the ones used in the histogram of the residuals shown in Fig. 3(c). The result is shown in Fig. 4, each point of which was made as shown in red in Fig. 3(a) with orders $-3 \le m \le 3$ using diffraction condition (13). The error bars reflect the uncertainty $\bar{\sigma}_{fit} = 1.8 \times 10^{-3}$ in the fit parameter a/λ based on the use of $\sigma_\theta = 1.4 \times 10^{-3}$ rad as the uncertainty associated with each angular measurement, as discussed above. The standard deviation of the seven measurements is $\sigma = 1.3 \times 10^{-3}$, somewhat smaller than the average uncertainty $\bar{\sigma}_{fit}$ of the individual measurements. A value of σ much larger than $\bar{\sigma}_{fit}$ might be suggestive of lattice distortion; here we see no such indication. The uncertainty in the mean of the measurements is thus [25] $\sigma_{mean} = \bar{\sigma}_{fit}/\sqrt{7} = 6.8 \times 10^{-4}$; in conjunction with the mean of the seven measurements,

Optics EXPRESS

we infer $a/\lambda = 2.3079(7)$. Taking the laser wavelength to be $\lambda = 632.816$ nm, we conclude that the lattice has a period of $a = 1460.5(3)$ nm.

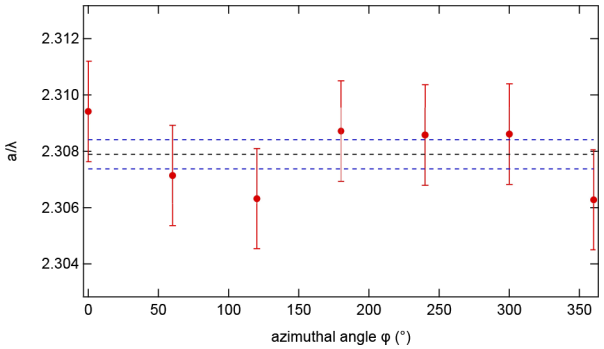

Fig. 4. Inferred value of a/λ for nominally equivalent azimuthal angles $\phi = N\pi/3$ for $0 \le N \le 6$; the first and last measurements are of the same actual angle. Error bars represent the uncertainty $\bar{\sigma}_{fit} = 1.8 \times 10^{-3}$ in a/λ deduced from the fit in each case. The dashed black line represents the average value of a/λ, equal to 2.3079; the standard deviation of the measurements is $\sigma = 1.3 \times 10^{-3}$. Interpreting the measurements as seven independent measurements of a/λ, the uncertainty (one standard deviation) of the mean is $\bar{\sigma}_{fit}/\sqrt{7} = 6.8 \times 10^{-4}$ (blue dashed lines).

A potential concern with measurements such as we have described is that the photonic crystal could be heated by the laser, thus leading to an erroneously high value of the measured period. The majority of the measurements described in this paper were made with an optical power of approximately 70 μW. To explore the possibility of laser-induced heating, we repeated a measurement of the hexagonal lattice, raising the optical power from $\approx 180\,\mu W$ to $\approx 480\,\mu W$ and back in steps of $\approx 100\,\mu W$. No systematic variation in the measurement of the period was observed.

5. Scanning electron microscope (SEM) measurements

To put our optical measurements in perspective, we now compare them to measurements made with an SEM, as discussed in the Introduction. Figure 5(a) shows an SEM image of a sample nominally identical to the hexagonal one whose measurements have been discussed above. We fit circles to each of the (complete) holes in the image to determine the centroids, and then calculated the nearest-neighbor distances along the six different directions given by $\theta = N\pi/6$, for $0<N<5$. We retained only those distances that did not share a circle, thus obtaining from 26 to 30 independent measurements of the period in these six directions. For each angle, the average of these measurements is shown in the blue squares in Fig. 5(b). These six points are scattered with a standard deviation of ≈ 6.4 nm, far greater than the uncertainties in the points themselves, clearly demonstrating image distortion. Similar measurements made at higher SEM magnifications are shown in Fig. 5(b) in red and green; they show the same trends but are not identical, confirming that they are caused by distortion and calibration issues in the SEM (and not the sample). Collectively, the SEM measurements have a standard deviation approximately twenty times larger than the uncertainty found with our Littrow diffraction approach, as well as an offset of approximately 20 nm.

Optics EXPRESS

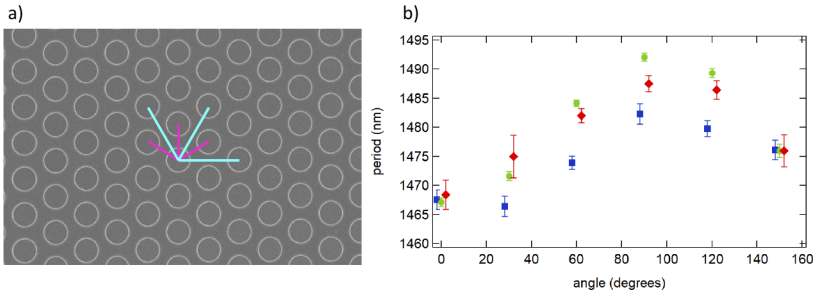

Fig. 5. a) SEM image of a sample nominally identical to the one studied in this work, at a magnification of 20 000 X. Measurements of the period are made from nearest-neighbor centroids along 30°, 90°, and 150° (magenta lines), and 0°, 60°, and 120° (cyan lines). For each angle, between $N = 26$ and $N = 30$ independent nearest-neighbor measurements can be made. **b)** Period inferred from independent nearest-neighbor distances for magnifications of 20 000 X (blue squares), 25 000 X (green circles), and 50 000 X (red diamonds), for the angles indicated at the left. The data points for different magnifications are slightly offset in the horizontal direction for clarity. Error bars represent the standard deviation of N independent measurements divided by $\sqrt{N-1}$. The image shows distortion at the 1 % level, somewhat dependent on the magnification used.

6. Conclusion

We have demonstrated a straightforward and robust approach to measuring the period of a photonic crystal slab with Littrow diffraction. The period is related to the wavelength of a reference laser by means of a simple equation in which the only two experimental parameters are the laser wavelength and the rotation angle; in practice the laser wavelength uncertainty is negligible, and the measurement uncertainty is dominated by the angular measurement. This approach is especially useful for photonic crystals aimed at telecom wavelengths or longer, in which light at a readily available visible wavelength will exhibit multiple orders of diffraction. Our measurements have yielded results with an uncertainty of ≈ 0.3 nm for crystals with both square and hexagonal lattices. Measurements made with an SEM, in contrast, show distortion that manifests itself in variations in the measured lattice constant of greater than 6 nm. The rotation stage we used was an inexpensive unit with a resolution of 5 arcmin, and all positioners were actuated manually. With better positioning stages, one should expect to obtain at least an order of magnitude of improvement in measurement accuracy. Our principal motivation for this work was to compare the performance of fabricated devices to simulations using high-fidelity geometric parameters, but the technique should also be useful to evaluate possible long-term variations in the lattice constant that could result from environmental conditions or sample aging.

Acknowledgments. The authors would like to thank Eric Shirley for useful discussions. Y. B. acknowledges support from the National Institute of Standards and Technology (NIST), Department of Commerce, USA (70NANB17H247). This research was performed in part in the NIST Center for Nanoscale Science and Technology Nanofab.

Disclosures. The authors declare no conflicts of interest.

Data availability. Data underlying the results presented in this paper are not publicly available at this time but may be obtained from the authors upon reasonable request.

References

1. J. Joannopoulos, S. Johnson, J. Winn, and R. Meade, *Photonic Crystals: Molding the Flow of Light* (Princeton University, 2008).
2. W. Zhou, D. Zhao, Y.-C. Shuai, H. Yang, S. Chuwongin, A. Chadha, J.-H. Seo, K. X. Wang, V. Liu, Z. Ma, and S. Fan, "Progress in 2D photonic crystal Fano resonance photonics," Prog. Quantum Electron. **38**(1), 1–74 (2014).
3. W. Suh and S. Fan, "All-pass transmission or flattop reflection filters using a single photonic crystal slab," Appl. Phys. Lett. **84**(24), 4905–4907 (2004).

Optics EXPRESS

4. S. Kim, S. Hadzialic, A. S. Sudbo, and O. Solgaard, "Reflectivity and polarization dependence of polysilicon single-film broadband photonic crystal micro-mirrors," Opt. Express **20**(6), 6306–6315 (2012).
5. B. Semnani, J. Flannery, R. Al Maruf, and M. Bajcsy, "Spin-preserving chiral photonic crystal mirror," Light: Sci. Appl. **9**(1), 23 (2020).
6. Y. Shuai, D. Zhao, Z. Tian, J.-H. Seo, D. V. Plant, Z. Ma, S. Fan, and W. Zhou, "Double-layer Fano resonance photonic crystal filters," Opt. Express **21**(21), 24582–24589 (2013).
7. C. Guo, M. Xiao, M. Minkov, Y. Shi, and S. Fan, "Isotropic wavevector domain image filters by a photonic crystal slab device," J. Opt. Soc. Am. A **35**(10), 1685–1691 (2018).
8. C. H. Bui, J. Zheng, S. W. Hoch, L. Y. T. Lee, J. G. E. Harris, and C. Wei Wong, "High-reflectivity, high- Q micromechanical membranes via guided resonances for enhanced optomechanical coupling," Appl. Phys. Lett. **100**(2), 021110 (2012).
9. X. Chen, C. Chardin, K. Makles, C. Caër, S. Chua, R. Braive, I. Robert-Philip, T. Briant, P.-F. Cohadon, A. Heidmann, T. Jacqmin, and S. Deléglise, "High-finesse Fabry–Perot cavities with bidimensional Si3N4 photonic-crystal slabs," Light: Sci. Appl. **6**(1), e16190 (2017).
10. H. Yang, D. Zhao, S. Chuwongin, J.-H. Seo, W. Yang, Y. Shuai, J. Berggren, M. Hammar, Z. Ma, and W. Zhou, "Transfer-printed stacked nanomembrane lasers on silicon," Nat. Photonics **6**(9), 615–620 (2012).
11. A. Kodigala, T. Lepetit, Q. Gu, B. Bahari, Y. Fainman, and B. Kanté, "Lasing action from photonic bound states in continuum," Nature **541**(7636), 196–199 (2017).
12. C. Jan, W. Jo, M. J. F. Digonnet, and O. Solgaard, "Photonic-crystal-based fiber hydrophone with sub-100 μPa/$\sqrt{\text{Hz}}$ pressure resolution," IEEE Photonics Technol. Lett. **28**(2), 123–126 (2016).
13. Y. Liu, S. Wang, P. Biswas, P. Palit, W. Zhou, and Y. Sun, "Optofluidic vapor sensing with free-space coupled 2D photonic crystal slabs," Sci. Rep. **9**(1), 4209 (2019).
14. C. R. Copeland, J. Geist, C. D. McGray, V. A. Aksyuk, J. A. Liddle, B. R. Ilic, and S. M. Stavis, "Subnanometer localization accuracy in widefield optical microscopy," Light: Sci. Appl. **7**(1), 31 (2018).
15. W. HäBler-Grohne and H. Bosse, "An electron optical metrology system for pattern placement measurements," Meas. Sci. Technol. **9**(7), 1120–1128 (1998).
16. C. P. Volk, E. S. Gornev, Y. A. Novikov, Y. V. Ozerin, Y. I. Plotnikov, and A. V. Rakov, "SEM Linear Measurement in a Wide Magnification Range," Russian Microelectron. **33**(6), 342–349 (2004).
17. M. T. Postek, "An approach to the reduction of hydrocarbon contamination in the scanning electron microscope," Scanning **18**(4), 269–274 (2006).
18. T. H. Yoon, C. I. Eom, M. S. Chung, and H. J. Kong, "Diffractometric methods for absolute measurement of diffraction-grating spacings," Opt. Lett. **24**(2), 107–109 (1999).
19. Q. Wang, Z. Liu, H. Chen, Y. Wang, X. Jiang, and S. Fu, "The method for measuring the groove density of variable-line-space gratings with elimination of the eccentricity effect," Rev. Sci. Instrum. **86**(2), 023109 (2015).
20. B. Sheng, G. Chen, Y. Huang, and L. Luo, "Measurement of grating groove density using multiple diffraction orders and one standard wavelength," Appl. Opt. **57**(10), 2514–2518 (2018).
21. T. Hof, D. Fick, and H. J. Jansch, "Application of diode lasers as a spectroscopic tool at 670 nm," Opt. Commun. **124**(3-4), 283–286 (1996).
22. E. Hecht and A. Zajac, *Optics* (Addison-Wesley Publishing Company, 1979).
23. N. W. Ashcroft and N. D. Mermin, *Solid State Physics* (Holt, Rinehart and Winston, 1976).
24. C. Kittel, *Introduction to Solid State Physics* (John Wiley and Sons, 1986).
25. J. R. Taylor, *An Introduction to Error Analysis* (University Science Books, 1997).

129.6.135.7 {ts '2022-09-22 14:49:23'}